

Charge Transport in Semiconductors Assembled from Nanocrystals

*Nuri Yazdani†, Samuel Andermatt‡, Maksym Yarema†, Vasco Farto†, Mohammad Hossein Bani-Hashemian‡, Sebastian Volk†, Weyde Lin†, Olesya Yarema†, Mathieu Luisier‡, Vanessa Wood†**

†Materials and Device Engineering Group, Department of Information Technology and

Electrical Engineering, ETH Zurich, Zurich CH-8092 Switzerland.

‡Nano TCAD Group, Department of Information Technology and Electrical Engineering, ETH

Zurich, Zurich CH-8092 Switzerland.

Quantum Dots, Nanocrystals, Polarons, Trap States, ...

Abstract

The potential of semiconductors assembled from nanocrystals (NC semiconductors) has been demonstrated for a broad array of electronic and optoelectronic devices, including transistors, light emitting diodes, solar cells, photodetectors, thermoelectrics, and phase charge memory cells. Despite the commercial success of nanocrystals as optical absorbers and emitters, applications involving charge transport through NC semiconductors have eluded exploitation due to the inability for predictive control of their electronic properties. Here, we perform large-scale, ab-

initio simulations to understand carrier transport, generation, and trapping in NC-based semiconductors from first principles. We use these findings to build the first predictive model for charge transport in NC semiconductors, which we validate experimentally. Our work reveals that we have been thinking about transport in NC semiconductors incorrectly. Our new insights provide a path for systematic engineering of NC semiconductors, which in fact offer previously unexplored opportunities for tunability not achievable in other semiconductor systems.

Main Text

Assembly of colloidal nanocrystals (NCs) into thin films¹ is envisaged as a means to achieve next generation, solution-processed semiconductors with electronic properties (e.g., band-gaps,² band-edge positions,³ mobilities,⁴ and free carrier densities⁵) that can be defined to match specific application requirements.^{6–10} This tunability is enabled by a multi-dimensional design space, where size, shape, composition, surface termination, and packing of the NCs can be systematically and independently controlled. While parametric studies have demonstrated some of the scaling relations in this design space,^{11–13} the fundamental mechanism driving charge transport in NC-based semiconductors has remained unclear, making it impossible to build a predictive model for charge transport in NC semiconductors or tap the full potential of NCs as building blocks for electronic materials through theory-guided design.

Here, we perform large-scale, *ab-initio* simulations to understand carrier transport, generation, and trapping in NC-based semiconductors from first principles. We use these findings to build and experimentally validate the first predictive model for charge transport in NC semiconductors. This predictive model allows us to design NC semiconductors with unique properties not achievable in

the bulk, and the fundamental insights into charge transport set a clear agenda for the development of NC chemistry and self-assembly to realize novel semiconductors.

Only recently has it been computationally feasible to treat the full atomic complexity of a NC *ab initio*, and this has proven key to understanding the mechanisms driving charge carrier dynamics on individual NCs.¹⁴ In order to elucidate the mechanisms for charge transport in NC-based semiconductors, we implement large-scale density functional theory (DFT) calculations on systems containing up to 125 NC (> 200000 atoms) (**Fig. 1a-b**).

As a model system, we use lead sulfide (PbS) NCs in the quantum confined regime (i.e., with radii $r < \sim 3$ nm) terminated with iodine ligands.¹⁵ Since NC size is a parameter that is easy to systematically control in experiments, we perform calculations for different sized NCs in order to validate the resulting charge transport model with experiments. Details are provided in the **Methods**.

Before we understand how charge moves across a NC-based semiconductor, we must first consider the impact of the presence of a charge carrier on an individual NC. To do so, we compute the ground state physical structure of the NCs in their neutral charge state and when charged. Upon charging with an electron (or hole), the Pb-iodine ligand bonds on the (111) surfaces of the NCs expand (or contract), while the Pb-S bond lengths remain unchanged (**Fig. 1c**, **Fig. S1**, and **Supporting Information note 1**). Thus, charge carriers on NCs are polarons. Because polarons result from electrostatic interaction of the charge carrier with the negatively charged ligands, polaron formation can be expected in any NC system with X-type ligands¹⁶ (e.g. halides, thiols, carboxylates).

Charge transfer from one NC to another thus implies a rearrangement of atoms at the surface of the two NCs. Although the shifts in bond length are small (up to 0.5 pm or 0.02% of the 3.22Å

nominal bond length), the associated reorganization energy for charge transfer between two NCs, λ , is large (10s to 100s of meV) (**Fig. 1d**). The reorganization energy decreases with increasing NC size due to a reduced carrier density across the NC and an increased number of ligands. In the **Supporting Information note 2**, we explain why it is reasonable to ignore the contribution to λ stemming from reorganization of the neighboring NCs (i.e., outer-shell reorganization).

Having now understood that charge on NCs forms polarons, we can determine the type of transport (band-like or hopping) by calculating the electronic coupling between neighboring nanocrystals, V_{ct} .

Since PbS NCs assemble into a body-centered-cubic, face-center-cubic, and related structures,¹⁷ we consider two relative orientations for neighboring NCs: [111]-neighbors and [100]-neighbors (**Fig. 1e**). We calculate electron and hole couplings for both orientations (i.e., V_{111} and V_{100}) over a range of r and inter-NC facet-to-facet distances, Δ_{ff} (**Fig. S2** and **Supporting Information note 3**). The results for $\Delta_{ff} = 6\text{\AA}$ are shown in **Fig. 1d**. V_{ct} increases strongly as the size of the NC decreases in agreement with analytical calculations modelling the NCs as spherical potential wells.¹⁸ This trend is explained by an increased carrier density on the outer atoms of the NC with increasing confinement in smaller NCs. The coupling in the [100] direction is about an order of magnitude larger than in the [111] direction, due to strong confinement of the carriers away from the ligand-rich [111] facets.¹⁴

The fact that V_{ct} is more than an order of magnitude smaller than λ over the range of r and Δ_{ff} of typical PbS NC-semiconductor informs us that the charge carriers, which are polarons, are localized on the individual NCs and that charge transport occurs through a phonon-assisted charge transfer (polaron hopping) between neighboring NCs.

Since the charge carrier deforms the Pb-ligand bonds upon polaron formation, charge transfer will be driven by the Pb-ligand vibrations. *Ab-initio* calculations of the phonon density-of-states of PbS NCs,¹⁴ backed by inelastic neutron¹⁹ and x-ray²⁰ scattering, indicate that Pb-ligand vibrations for common X-type ligands occur at energies $\hbar\omega < \sim 15$ meV. Therefore, at temperatures above ~ 175 K, charge transfer will occur at a rate:²¹

$$k_{ct} = N_P \frac{2\pi}{\hbar} V_{ct}^2 \sqrt{\frac{1}{4\pi\lambda k_B T}} e^{-(\Delta E + \lambda)^2 / 4\lambda k_B T}, \quad (1)$$

where $\Delta E = E_P - E_R$ (i.e. the energy of the products minus the energy of the reactants) and N_P is the number of degenerate product states (**Fig. 1f**). At temperatures below ~ 175 K, transfer rates will saturate to their temperature-independent, low temperature limit (**Supporting Information note 4**), or, in the presence of disorder, transport will transition to an Efros-Shlovskii variable range hopping regime.²²

Assuming a NC-semiconductor of isoenergetic NCs and no applied field ($\Delta E = 0$), **Eq. 1** predicts charge transfer rates on the order of 10-100s ps for PbS NC-semiconductors at room temperature, in agreement with recent measurements.¹³ Since intra-band carrier cooling rates in PbS NCs proceed at 100s fs times scales,²³ the reactant and product states are thus the highest occupied electronic states (in the case of hole transport) or the lowest unoccupied electronic states (in the case of electron transport). This is in agreement with experimental measurement of the mobility band gap in a NC-semiconductor scaling linear with the band gap of the individual NCs.²⁴

In a realistic NC-semiconductor, $\Delta E \neq 0$, with differences in the alignment between the highest occupied (or lowest unoccupied) states of neighboring NCs contributing to ΔE . Since a large ΔE will have significant impact on the time scales of transport, it is therefore critical to understand and control the energetic landscape within a NC solid. One contribution to ΔE is the distribution of the individual NC bandgaps, stemming from size and shape disorder of the constituent NCs.

Additionally, deep, electronic trap states are known to exist in NC-semiconductors,²⁵ and possible explanations of their origin include mid-gap states on individual NCs²⁶ and fused NC dimers.²⁷ Here, we demonstrate oxidized or reduced doped NCs in the NC-semiconductor also form electronic traps in NC-semiconductors.

An individual NC is doped according to the oxidation-number sum rule:^{28,29}

$$N_C V_C + N_A V_A + \sum_i V_i = \begin{cases} 0, & \text{intrinsic,} \\ < 0, & \text{p-doped,} \\ > 0, & \text{n-doped,} \end{cases} \quad (2)$$

where N_x is the number of the cations (C) and anions (A), and I are the impurities and ligands with valence V_x comprising the NC. Doped NCs will in general be energetically unfavorable; however, small densities of doped-NCs are to be expected through reaction kinetics.²⁹ For PbS-NCs for example, an excess of Pb during synthesis can lead to a small fraction of n -doped PbS NCs, and exposure of PbS NC-semiconductors to oxygen leads to p -doping.

We compute the electronic structure of a NC-semiconductor containing a single n -doped NC surrounded by intrinsic NCs (**Fig. 2a**). For reference, the electronic structures of isolated intrinsic, n -doped, and oxidized n -doped NC (with net charge e^+) are shown in **Fig. 2b**. In a NC semiconductor, if the n -doped NC is not oxidized, its energy levels remain aligned with those of the neighboring intrinsic NCs (**Fig. 2c**). However, oxidation causes a shift in the energy levels of the n -doped NC as well as its neighbors (**Fig. 2c, Fig. S3**).

Within a NC-semiconductor, oxidized n -doped NCs thus behave as electronic traps for electrons and as barriers for hole transport. Equivalently, reduced p -doped nanocrystals present traps for holes and barriers for electrons (**Fig. S4**). Defining the trap depth ($E_T(r, \Delta\mu)$) as the extent of the shift of energy level in an oxidized or reduced doped NC relative to a NC infinitely far from the doped NC (**Fig. 2d, Fig. S5**), we find that our calculated trap depths agree with the experimentally

measured trap depths^{19,24} as well as the charging energy of the NCs computed using the measured size-dependent dielectric constant for PbS NC-semiconductors.³⁰ Thus, while trap states have been typically ascribed to mid-gap electronic states on individual NCs, they are in fact, charged, doped-NCs in a NC-semiconductor.

In this picture, trapping and release of charge carriers from traps is thus simply phonon-assisted charge transfer between the highest occupied or lowest unoccupied states of neighboring NCs with rates given by **Eq. 1**, where $E_T(r, \Delta\mu)$ is included in ΔE . Doing so results in release rates on the order of 10^2 for $r = 1$ nm NCs and up to 10^8 for $r = 3$ nm, in agreement with the rates characterized previously with thermal-admittance-spectroscopy¹⁹ (see **Fig. S6**).

These results also indicate that the excess carrier on a doped NC must overcome a large energetic barrier (equal to E_T) to become a free carrier in the NC-semiconductor. Particularly in small NCs, where E_T is large, free carrier densities in NC-based semiconductors will be negligible even when large densities of doped-NCs are present. For example, for a semiconductor made of $r = 1.6$ nm PbS NCs, assuming 1% of NCs are *n*-doped, the free electron density at room temperature will be $\sim 10^{12}$ cm⁻³, in stark contrast to the total density of *n*-doped NCs, $\sim 10^{16}$ cm⁻³. However, the formation of a space-charge region can lead to oxidation (or reduction) of the doped NCs, resulting in high trap densities.

To summarize, our large-scale DFT calculations provide several key insights into charge transport in semiconductors assembled from NCs: 1) charge on individual NCs forms polarons, 2) charge transport occurs via phonon-mediated charge transfer, and 3) oxidized or reduced doped-NCs become electronic traps states within the NC-semiconductor.

We experimentally validate these insights into charge transport in NC-based semiconductors by performing time-of-flight (TOF) photocurrent transient measurements⁴ (see **Methods, Fig. S7**). In

a TOF measurement, a laser pulse generates a low density of charge carriers in the NC-semiconductor (**Fig. 3a**), and the displacement current generated by the electrons or holes traversing the film of thickness d is measured for a range of biases across the device, V_B , at temperatures $T \sim 220 - 330\text{K}$ (**Fig. 3b**). The resulting transients can be fit with two distinct power laws at short and long times (**Fig. 3b**), with their intersection taken as an effective transit time, $t_{tr}(V_B, T)$. $t_{tr}(V_B, T)$ corresponds to the maximum of the statistical distribution of carrier transport times across the device, and, by fitting $t_{tr}(V_B, T)$ simultaneously for all temperatures T and biases V_B (**Fig. 3c**), it is possible to extract an effective mobility, μ_{eff} :

$$\frac{d}{t_{tr}(V, T)} = \mu_{eff}(r, \Delta_{ff}, T) \frac{(V_B + V_{B0})}{d}, \quad (3)$$

where V_{B0} is the built-in field in the device. The long-time portion of the transient reflects the large dispersion in carrier transit times, and are discussed further in **Supporting Information note 6**.

We first note that, in the limit that the potential drop across neighboring NCs is smaller than the reorganization energy ($(V_B + V_{B0})(2r + \Delta_{ff})/d \ll \lambda$), we can use **Eq. 1** to write:

$$\mu_{eff}(r, \Delta_{ff}, T) = N_p \frac{2\pi}{h} \frac{V_{ct}^2}{\lambda^{1/2}} \frac{(2r + \Delta_{ff})^2}{2k_B T} \sqrt{\frac{1}{4\pi k_B T}} e^{-E_A/k_B T}. \quad (4)$$

and thereby extract V_{ct} and E_A from experiment (**Fig. S8**). We find good agreement between the experimentally extracted V_{e^*} and V_{h^*} and computed values for electron and hole coupling in the [100] direction (**Fig. 3d**). The extracted activation energies, which range from 70 meV to 150 meV (**Fig. 3e**), are larger than those expected for a NC-semiconductor with no energetic disorder ($E_A = \lambda/4 \sim 10$ meV to 40 meV) (**Fig. 1d**). Instead, the activation energies are consistent with the values expected when electronic traps dominate the timescales of carrier transport. The fact that the electronic coupling V_{ct} measured in this trap-limited transport regime agrees with our calculations

of V_{ct} between neighboring NCs indicate that the trap states limiting the effective mobility in NC-based semiconductors are those stemming from oxidized (or reduced) doped-NCs.

Confident in our new understanding of charge-transport in NC-based semiconductor, we build a Kinetic Monte Carlo (KMC) simulation of polaron transport, which we parameterize with the DFT calculated values for electronic coupling V_{ct} , reorganization energy λ , and electronic trap depth E_T (See **Methods**). In this multiscale model, charge transport across a NC-based semiconductor is simulated as sequential charge transfers between neighboring NCs i and j . The rate of charge transfer is k_{ij} (which is given by **Eq. 1**) with energy offset between neighboring NCs, ΔE_{ij} , is taken as

$$\Delta E_{ij} = (E_{g,j} - E_{g,i})/2 - \vec{E}_z \cdot (\vec{r}_j - \vec{r}_i), \quad (5)$$

where $E_{g,i}$ is the band-gap of NC i , E_z is the electric field across the NC-semiconductor (assumed to be in the z -direction), and r_i are the coordinates of NCs. For our simulation, we construct artificial NC semiconductors having the thicknesses and containing the different sized NCs that are investigated experimentally with TOF, and simulate current transients for different biases, carrier types (electrons and holes), and temperatures. Only the density of trap states as a function of NC size, $p\tau(r)$, is left as a free parameter (**Supporting Information note 7**). The examples shown in **Fig. 4a** highlight that all simulated transients (red lines) match the measured transients (blue lines), both the effective mobilities defined by $t_{tr}(V_B, T)$, as well as the long-time ($t > t_{tr}(V_B, T)$) dispersion of the transients. We find trap states densities selected to achieve agreement are within the expected range, and otherwise, no fitting is carried out to achieve the agreement between the simulated and experimental current transient measurements.

This predictive, multiscale model can be used to systematically design next generation NC-based semiconductors. Here, we consider how to overcome one intrinsic limitation we identified, namely

the one-to-one correspondence between the free carrier generation in a NC and the formation of deep traps.

In **Fig. 4b**, we plot the simulated relative mobility of a PbS NC-semiconductor, (μ_{eff} / μ_0) , defined by the time required for $\sim 63\%$ of the carriers to traverse a 400 nm-thick film, as a function of bandgap disorder σ_{Eg} and trap density ρ_T , relative to that for a trap- and disorder-free NC-semiconductor, μ_0 . While band-gap disorder has a similar impact on carrier mobility for both small and large NCs, the impact of deep traps can most easily be mitigated by using larger NCs, or by significantly decreasing Δ_{ff} (e.g. through epitaxially connected NC-semiconductors¹¹) since $E_T(r, \Delta_{ff})$ decreases with increasing r and decreasing Δ_{ff} .

Our insights enable us to identify a more flexible approach: a NC semiconductor composed of intrinsic NCs can be doped with p- or n-doped NCs with bandgaps larger than that of the intrinsic NCs. With proper selection of bandgap, the shifted highest occupied state of oxidized *p*-doped NCs or the lowest unoccupied state of reduced *n*-doped NCs will align with the highest occupied states or lowest unoccupied states of the intrinsic NCs (**Fig. 4c**). This simultaneously eliminates deep traps and energetic barriers for thermal release of carriers, and leads to multiple orders of magnitude higher mobilities and free carrier densities. Such a strategy can be achieved with a bimodal size distribution of NCs or with equal-sized doped NCs of a different core material (and thus different bandgaps).

In summary, our insights highlight the need to reframe how we think about charge transport, trapping, and doping in NC semiconductors. The fact that charge transport in NC-semiconductors occurs via phonon-mediated charge transfer suggests that, when it comes to transport, we should view NC not as small, quantized pieces of a bulk semiconductor, but rather as large molecules, where polaron-hopping transport dominates. Indeed, from this perspective NCs semiconductors

present highly tunable systems that offer complete control of electronic coupling through tuning of the electronic confinement in the individual NC, the spacing, and the topology of the NC lattice, as well as the activation energies associated with transport through tuning of the NC dispersity, doping, and surfaces. By controlling the phonon densities-of-states and electron-phonon coupling through atomic engineering of the NCs and their surfaces, the rates and temperature-dependences of transport can also be systematically tuned. The example of PbS NC-based semiconductors illustrates how it is possible to engineer electronic anisotropies into semiconductors (i.e., transport in [100] will be faster than in [111]), without resorting to anisotropic crystal structures. This enables the creation of semiconductors with isotropic optical properties but with highly anisotropic electronic properties (as in the case of PbS), or with highly anisotropic optical properties and highly isotropic electronic properties. These findings position NC semiconductors not only as highly tunable, solution-processed semiconductors but also as model, tunable systems for studying the fundamental physics of charge transfer processes.

ASSOCIATED CONTENT

Supporting Information

The Supporting Information is available free of charge on the ACS Publications website at DOI: 10.1021/acs.nano-lett.XXXXX

AUTHOR INFORMATION

Corresponding Author

*E-mail: vwood@ethz.ch.

Author Contributions

N.Y. and V.W. devised the work, N.Y. performed all modelling and calculations, with input from S.A., M.H.B.-H., and M.L. for the trap depth calculations, N.Y. fabricated heterojunction devices with materials synthesized by M.Y. and O.Y., using setups maintained by S.V. and W.M.M.L., V.F. and N.Y. fabricated the inverted heterojunction devices, N.Y. performed the TOF experiments and analyzed results, N.Y. and V.W. wrote the manuscript with input from all other authors.

ACKNOWLEDGMENT

The authors acknowledge an ETH Research Grant (N.Y), the Swiss National Science Foundation Quantum Sciences and Technology NCCR (N.Y.). Computations were supported by grants from the Swiss National Supercomputing Centre (CSCS; project IDs s674, s831, s876).

REFERENCES

- (1) Kagan, C. R.; Lifshitz, E.; Sargent, E. H.; Talapin, D. V. Building Devices from Colloidal Quantum Dots. *Science* **2016**, 353 (6302), aac5523–aac5523. <https://doi.org/10.1126/science.aac5523>.
- (2) Talapin, D. V; Lee, J.-S.; Kovalenko, M. V; Shevchenko, E. V. Prospects of Colloidal Nanocrystals for Electronic and Optoelectronic Applications. *Chem. Rev.* **2010**, 110 (1), 389–458. <https://doi.org/10.1021/cr900137k>.
- (3) Brown, P. R.; Kim, D.; Lunt, R. R.; Zhao, N.; Bawendi, M. G.; Grossman, J. C.; Bulovi??, V. Energy Level Modification in Lead Sulfide Quantum Dot Thin Films through Ligand Exchange. *ACS Nano* **2014**, 8 (6), 5863–5872. <https://doi.org/10.1021/nn500897c>.
- (4) Yazdani, N. A.; Bozyigit, D.; Yarema, O.; Yarema, M.; Wood, V. Hole Mobility in

- Nanocrystal Solids as a Function of Constituent Nanocrystal Size. *J. Phys. Chem. Lett.* **2014**, 5 (20), 3522–3527. <https://doi.org/10.1021/jz5015086>.
- (5) Cargnello, M.; Johnston-Peck, A. C.; Diroll, B. T.; Wong, E.; Datta, B.; Damodhar, D.; Doan-Nguyen, V. V. T.; Herzing, A. A.; Kagan, C. R.; Murray, C. B. Substitutional Doping in Nanocrystal Superlattices. *Nature* **2015**, 524 (7566), 450–453. <https://doi.org/10.1038/nature14872>.
 - (6) Swarnkar, A.; Marshall, A. R.; Sanhira, E. M.; Chernomordik, B. D.; Moore, D. T.; Christians, J. A.; Chakrabarti, T.; Luther, J. M. Quantum Dot-Induced Phase Stabilization of -CsPbI₃ Perovskite for High-Efficiency Photovoltaics. *Science* **2016**, 354 (6308), 92–95. <https://doi.org/10.1126/science.aag2700>.
 - (7) Fan, F.; Voznyy, O.; Sabatini, R. P.; Bicanic, K. T.; Adachi, M. M.; McBride, J. R.; Reid, K. R.; Park, Y. S.; Li, X.; Jain, A.; et al. Continuous-Wave Lasing in Colloidal Quantum Dot Solids Enabled by Facet-Selective Epitaxy. *Nature* **2017**, 544 (7648), 75–79. <https://doi.org/10.1038/nature21424>.
 - (8) Ackerman, M. M.; Tang, X.; Guyot-Sionnest, P. Fast and Sensitive Colloidal Quantum Dot Mid-Wave Infrared Photodetectors. *ACS Nano* **2018**, 12 (7), 7264–7271. <https://doi.org/10.1021/acsnano.8b03425>.
 - (9) Lim, J.; Park, Y.-S.; Klimov, V. I. Optical Gain in Colloidal Quantum Dots Achieved with Direct-Current Electrical Pumping. *Nat. Mater.* **2017**, 17 (1), 42–49. <https://doi.org/10.1038/nmat5011>.
 - (10) Rainò, G.; Becker, M. A.; Bodnarchuk, M. I.; Mahrt, rainer F.; Kovalenko, M. V; Stöferle,

- T. Superfluorescence from Lead Halide Perovskite Quantum Dot Superlattices. *Nature* **2018**, *563* (7733), 671–675. <https://doi.org/10.1038/s41586-018-0683-0>.
- (11) Whitham, K.; Yang, J.; Savitzky, B. H.; Kourkoutis, L. F.; Wise, F.; Hanrath, T. Charge Transport and Localization in Atomically Coherent Quantum Dot Solids. *Nat. Mater.* **2016**, *15* (5), 557–563. <https://doi.org/10.1038/nmat4576>.
- (12) Gilmore, R. H.; Winslow, S. W.; Lee, E. M. Y.; Ashner, M. N.; Yager, K. G.; Willard, A. P.; Tisdale, W. A. Inverse Temperature Dependence of Charge Carrier Hopping in Quantum Dot Solids. *ACS Nano* **2018**, *12* (8), 7741–7749. <https://doi.org/10.1021/acsnano.8b01643>.
- (13) Proppe, A. H.; Xu, J.; Sabatini, R. P.; Fan, J. Z.; Sun, B.; Hoogland, S.; Kelley, S. O.; Voznyy, O.; Sargent, E. H. Picosecond Charge Transfer and Long Carrier Diffusion Lengths in Colloidal Quantum Dot Solids. *Nano Lett.* **2018**, *18* (11), 7052–7059. <https://doi.org/10.1021/acs.nanolett.8b03020>.
- (14) Yazdani, N.; Bozyigit, D.; Vuttivorakulchai, K.; Luisier, M.; Infante, I.; Wood, V. Tuning Electron–Phonon Interactions in Nanocrystals through Surface Termination. *Nano Lett.* **2018**, *18* (4), 2233–2242. <https://doi.org/10.1021/acs.nanolett.7b04729>.
- (15) Zharebetsky, D.; Scheele, M.; Zhang, Y.; Bronstein, N.; Thompson, C.; Britt, D.; Salmeron, M.; Alivisatos, P.; Wang, L.-W. Hydroxylation of the Surface of PbS Nanocrystals Passivated with Oleic Acid. (Suppl Mat). *Science* **2014**, *344* (6190), 1380–1384. <https://doi.org/10.1126/science.1252727>.
- (16) Owen, J. The Coordination Chemistry of Nanocrystal Surfaces. *Science* **2015**, *347* (6222), 615–616. <https://doi.org/10.1126/science.1259924>.

- (17) Weidman, M. C.; Smilgies, D.-M.; Tisdale, W. A. Kinetics of the Self-Assembly of Nanocrystal Superlattices Measured by Real-Time in Situ X-Ray Scattering. *Nat. Mater.* **2016**, *15* (March), 1–8. <https://doi.org/10.1038/nmat4600>.
- (18) Shabaev, A.; Efros, A. L.; Efros, A. L. Dark and Photo-Conductivity in Ordered Array of Nanocrystals. *Nano Lett.* **2013**, *13* (11), 5454–5461. <https://doi.org/10.1021/nl403033f>.
- (19) Bozyigit, D.; Yazdani, N.; Yarema, M.; Yarema, O.; Lin, W. M. M.; Volk, S.; Vuttivorakulchai, K.; Luisier, M.; Juranyi, F.; Wood, V. Soft Surfaces of Nanomaterials Enable Strong Phonon Interactions. *Nature* **2016**, *531* (7596), 618–622. <https://doi.org/10.1038/nature16977>.
- (20) Yazdani, N.; Nguyen-Thanh, T.; Yarema, M.; Lin, W. M. M.; Gao, R.; Yarema, O.; Bosak, A.; Wood, V. Measuring the Vibrational Density of States of Nanocrystal-Based Thin Films with Inelastic X-Ray Scattering. *J. Phys. Chem. Lett.* **2018**, *9* (7), 1561–1567. <https://doi.org/10.1021/acs.jpclett.8b00409>.
- (21) Bixon, M.; Jortner, J. Electron Transfer—from Isolated Molecules to Biomolecules. In *Advances in Chemical Physics*; 1999; pp 35–202. <https://doi.org/10.1002/9780470141656.ch3>.
- (22) Erslev, P. T.; Chen, H.-Y.; Gao, J.; Beard, M. C.; Frank, A. J.; van de Lagemaat, J.; Johnson, J. C.; Luther, J. M. Sharp Exponential Band Tails in Highly Disordered Lead Sulfide Quantum Dot Arrays. *Phys. Rev. B* **2012**, *86* (15), 155313. <https://doi.org/10.1103/PhysRevB.86.155313>.
- (23) Spoor, F. C. M.; Kunneman, L. T.; Evers, W. H.; Renaud, N.; Grozema, F. C.; Houtepen,

- A. J.; Siebbeles, L. D. A. Hole Cooling Is Much Faster than Electron Cooling in PbSe Quantum Dots. *ACS Nano* **2016**, *10* (1), 695–703. <https://doi.org/10.1021/acsnano.5b05731>.
- (24) Bozyigit, D.; Lin, W. M. M. M.; Yazdani, N.; Yarema, O.; Wood, V. A Quantitative Model for Charge Carrier Transport, Trapping and Recombination in Nanocrystal-Based Solar Cells. *Nat. Commun.* **2015**, *6* (1), 6180. <https://doi.org/10.1038/ncomms7180>.
- (25) Nagpal, P.; Klimov, V. I. Role of Mid-Gap States in Charge Transport and Photoconductivity in Semiconductor Nanocrystal Films. *Nat. Commun.* **2011**, *2*, 486. <https://doi.org/10.1038/ncomms1492>.
- (26) Katsiev, K.; Ip, A. H.; Fischer, A.; Tanabe, I.; Zhang, X.; Kirmani, A. R.; Voznyy, O.; Rollny, L. R.; Chou, K. W.; Thon, S. M.; et al. The Complete In-Gap Electronic Structure of Colloidal Quantum Dot Solids and Its Correlation with Electronic Transport and Photovoltaic Performance. *Adv. Mater.* **2014**, *26* (6), 937–942. <https://doi.org/10.1002/adma.201304166>.
- (27) Gilmore, R. H.; Liu, Y.; Shcherbakov-Wu, W.; Dahod, N. S.; Lee, E. M. Y.; Weidman, M. C.; Li, H.; Jean, J.; Bulović, V.; Willard, A. P.; et al. Epitaxial Dimers and Auger-Assisted Detrapping in PbS Quantum Dot Solids. *Matter* **2019**, *1* (1), 250–265. <https://doi.org/10.1016/j.matt.2019.05.015>.
- (28) Sluydts, M.; De Nolf, K.; Van Speybroeck, V.; Cottenier, S.; Hens, Z. Ligand Addition Energies and the Stoichiometry of Colloidal Nanocrystals. *ACS Nano* **2016**, *10* (1), 1462–1474. <https://doi.org/10.1021/acsnano.5b06965>.

- (29) Voznyy, O.; Zhitomirsky, D.; Stadler, P.; Ning, Z.; Hoogland, S.; Sargent, E. H. A Charge-Orbital Balance Picture of Doping in Colloidal Quantum Dot Solids. *ACS Nano* **2012**, 6 (9), 8448–8455. <https://doi.org/10.1021/nn303364d>.
- (30) Grinolds, D. D. W.; Brown, P. R.; Harris, D. K.; Bulovic, V.; Bawendi, M. G. Quantum-Dot Size and Thin-Film Dielectric Constant: Precision Measurement and Disparity with Simple Models. *Nano Lett.* **2015**, 15 (1), 21–26. <https://doi.org/10.1021/nl5024244>.

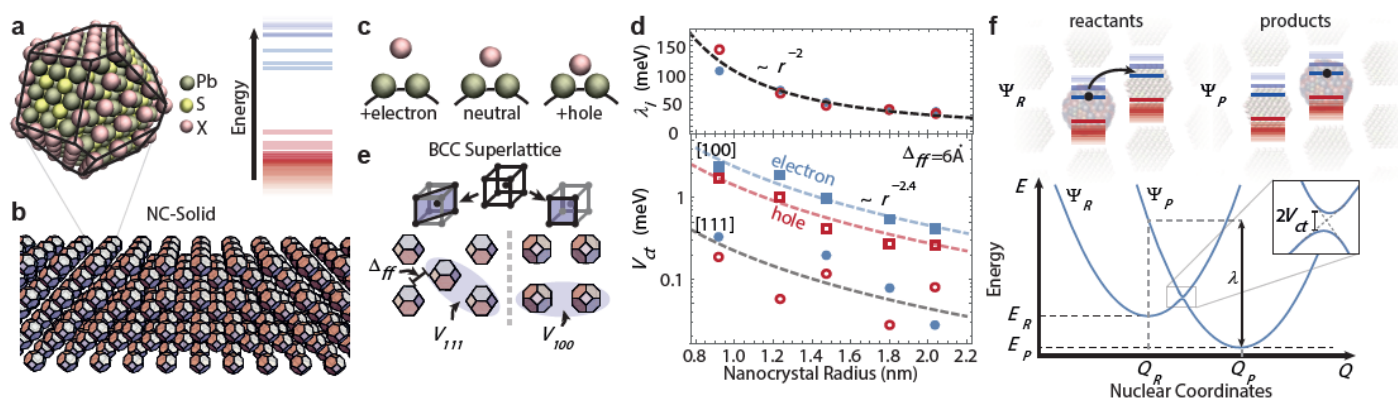


Fig. 1 Charge Transfer in NC-solids (a) Atomistic model of a PbS nanocrystal (NC) with halide (I) surface passivation and its quantized electronic structure. (b) Depiction of a thin film of nanocrystals (i.e., a NC solid). (c) Schematic of the nuclear reorganization, where the Pb-X bonds on the surface of the NC expand or shrink in the presence of an electron or hole. (d) Calculated reorganization energy (top) and electronic coupling (bottom) for electrons (blue) or holes (red) between [100] (squares) and [111] (circles) nearest neighbors (as depicted in (e)), assuming a facet-to-facet distance, Δ_{ff} , of 6 Å in the [111] direction. (f) Configurational diagram for charge transfer between two nanocrystals, where an electron (black dot) moves from the nanocrystal on the left (configuration of reactants, Q_R , with ground state energy E_R) to the nanocrystal on the right (Q_P and energy E_R). The reorganization energy (λ) and electronic coupling (V_{CT}) is shown graphically.

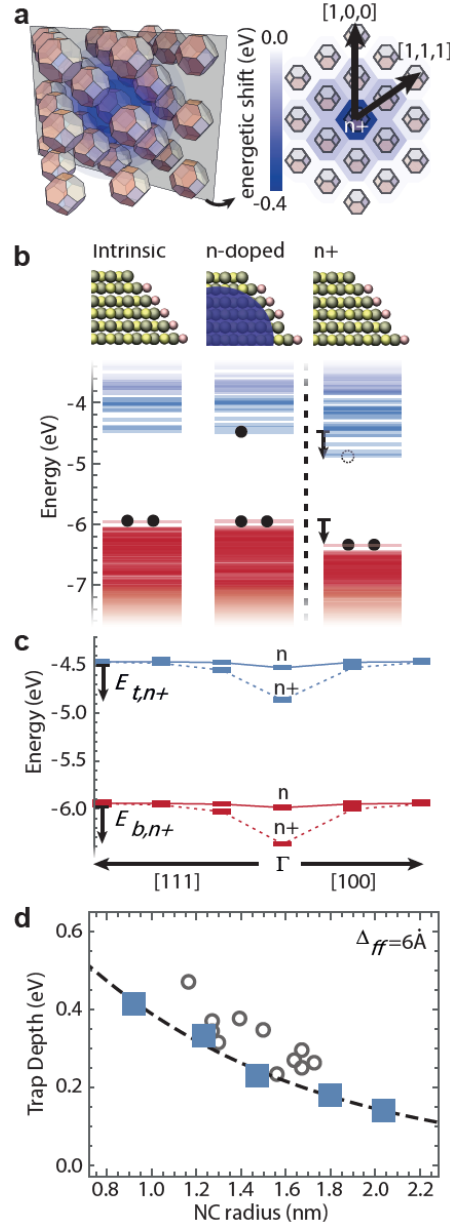


Fig. 2 Origin of deep traps in NC-solids. (a) A schematic representation of an $n+$ or $p-$ NC in a solid of intrinsic NCs, where the shift in the energy structure will be screened by neighboring NCs. (b) Contour plot of the energy shifts of the lowest unoccupied electronic level in NCs ($r = 0.95$ nm with $\Delta_{ff} = 0.6$ Å) for an $n+$ NC in an NC solid. (c) Electronic structure of intrinsic, n-doped, and oxidized n-doped NC ($n+$). (d) Highest occupied electronic levels (red) and lowest unoccupied electronic levels (blue) of an n , $n+$ NC at the Γ point in the BCC lattice and its intrinsic neighbors in the $[111]$ and $[100]$ directions in a NC-solid. (e) Trap depth as a function of NC size for NCs in vacuum (circles) and for NC-solids (squares). Experimentally measured trap depths on PbS NC-solids (19, 24) (gray circles) and the NC charging energies calculated for a sphere of radius r in a PbS NC-solid (dashed gray line) (see **Supplementary Materials note 5**).

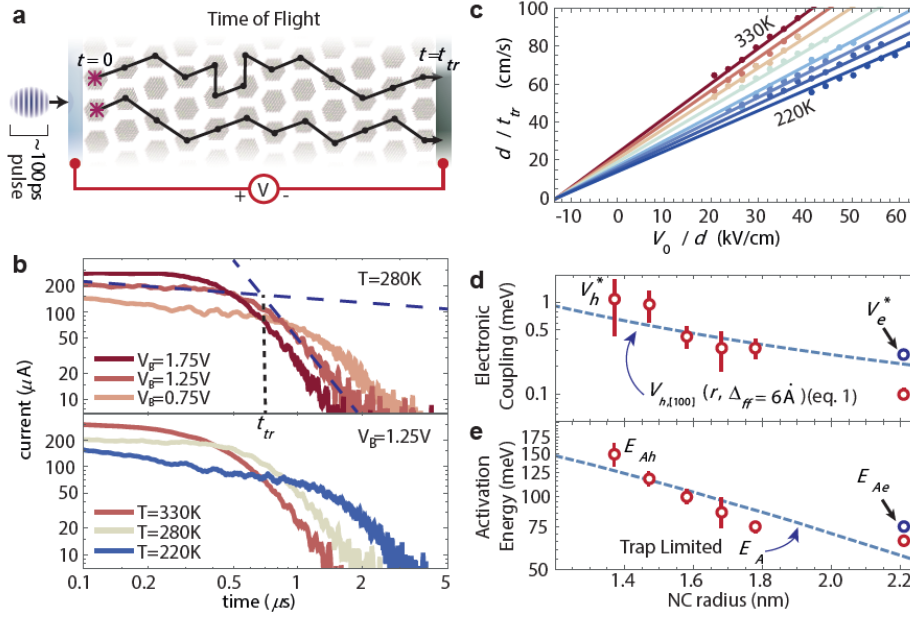


Fig. 3 Trap-Limited Transport in NC-solid. (a) Schematic of time-of-flight (TOF) photocurrent transient measurements. (b) Hole transients measured at various biases and temperatures on a NC-solid ($r_{NC} = 2.21$ nm). (c) Plot of the hole velocity, d/t_{tr} , versus applied field, V_B/d , at various temperatures. Solid lines indicate the fit to eq. 4. (d) Electronic coupling and (e) activation energy extracted from TOF measurements as a function of the NC radius r compared to computed $V_{h[100]}$ and E_A assuming trap limited transport (dashed lines).

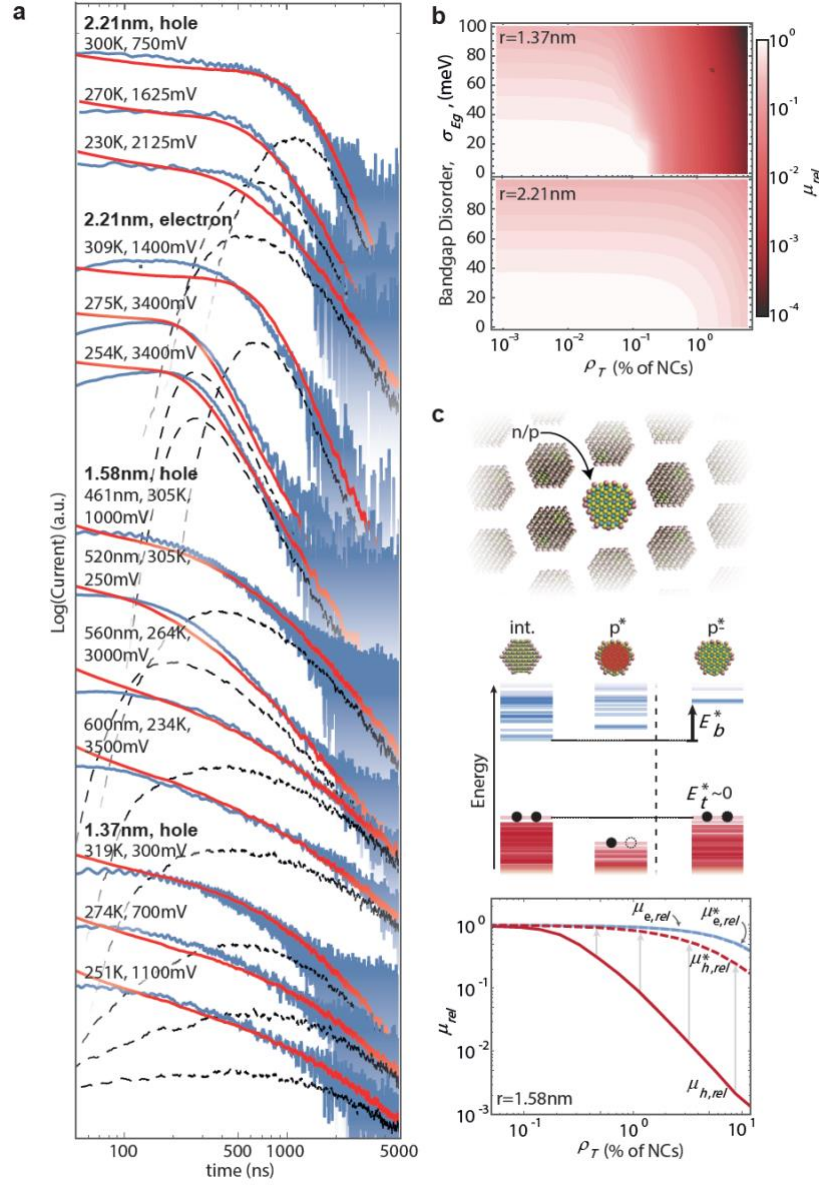


Fig. 4 Predictive Model for Charge Transport (a) Measured TOF transients (blue) and Kinetic Monte Carlo (KMC) simulated transients (red) are shown for various NC sizes, temperatures, biases, and device thicknesses. Distribution of carrier transit times from the simulated transients (dashed black line). (b) Plot of the ratio of the effective mobility as a function of trap density ρ_T and NC bandgap disorder σ_{Eg} to the effective mobility of a trap and disorder free NC-solid for smaller (top) and larger (bottom) NC sizes, calculated for a 400nm-thick NC-solid at 300K (c) Doping without the formation of trap states can be achieved by introduction of larger-bandgap, n - or p -doped NCs. Simulations demonstrate that this prevents a decrease in effective mobility at high carrier concentrations.

TOC graphic

